



Synthesis of highly crystalline rhombohedral BN triangular nanoplates via a convenient solid state reaction

Keyan Bao^a, Fengyang Yu^b, Liang Shi^a, Shuzhen Liu^a, Xiaobo Hu^a, Jie Cao^a, Yitai Qian^{a,*}

^a Department of Chemistry, Hefei National Laboratory for Physical Sciences at Microscale, University of Science and Technology of China, Hefei, Anhui 230026, PR China

^b Department of Basic Science, Tianjin Agriculture University, Tianjin 300384, PR China

ARTICLE INFO

Article history:

Received 8 July 2008

Received in revised form

6 January 2009

Accepted 7 January 2009

Available online 19 January 2009

Keywords:

BN

Rhombohedral

Triangular nanoplates

TGA

PL

ABSTRACT

Highly crystalline rhombohedral boron nitride (r-BN) with regular triangular shapes were synthesized on a large scale in a stainless steel autoclave using B_2O_3 and $NaNH_2$ as reactants at 600 °C for 6 h. The as-prepared BN triangular nanoplates have an average edge length of 400 nm and the thickness of about 60 nm. The photoluminescence measurements reveal that the r-BN products show strong yellow-green emission. The as-prepared r-BN has potential optical and optoelectronic applications in high temperature devices due to its excellent thermal stability and anti-oxidation properties.

© 2009 Elsevier Inc. All rights reserved.

1. Introduction

Boron nitride (BN) has attracted much interest due to its unique physical and chemical properties, such as low density, high temperature stability, high thermal conductivity, high melting point and low dielectric constant. Owing to these properties, boron nitride can be used as lubricants, electrical insulators, refractory [1–4]. Usually, BN has four polymorphs with well-defined crystallographic structures, including two high-density diamond-like phases: cubic BN (c-BN), wurtzite BN (w-BN) and two low-density graphite-like phases: hexagonal BN (h-BN), rhombohedral BN (r-BN) [2]. All BN forms have a wide bandgap, making it a promising candidate for deep-blue and UV applications [5].

Up to now, h-BN nanomaterials with various shapes have been prepared, including nanotubes [6,7], nanocapsules [8], nanoparticles [9], hollow spheres [10–12], needle-like nanocrystals [13], and nanoropes [14]. C-BN nanoparticles [15–22] have also been synthesized. However, the preparations of r-BN and w-BN nanostructures are relatively rare. So far, r-BN nanoparticles were obtained by a chemical vapor deposition method from $BCl_3-NH_3-H_2$ gas system at 1600 °C [23]. Nanobamboo structure of r-BN was synthesized from the reaction of barium metaborate with ammonia at 1300 °C [24]. A mixture of hexagonal and rhombohedral BN nanotubes was synthesized by CVD method

[25]. Crystalline r-BN triangular nanoplates were produced by means of a Ni-catalyzed route at 600 °C [26]. However, in the absence of Ni only BN particles were obtained.

In this study, we reported a facile chemical route for the synthesis of highly crystalline r-BN triangular nanoplates without using any catalyst or templates. The r-BN triangular nanoplates were prepared via the reaction of B_2O_3 and $NaNH_2$ in an autoclave at 600 °C for 6 h. The intermediate process in the formation of r-BN triangular nanoplates was investigated and the possible growth mechanism has been discussed. The products have been characterized by means of X-ray diffraction (XRD), field emission scanning electron microscope (FESEM), high-resolution transmission electron microscopy (HRTEM), selected area electron diffraction (SAED), thermogravimetric-differential analysis (TGA-DTA), and photoluminescence (PL) measurements. The as-synthesized products exhibit excellent luminescence, thermal stability and anti-oxidation properties, which extend their potential optical and optoelectronic applications to the field of high temperature devices.

2. Experimental

All the chemical reagents were obtained from Shanghai Chemical Co. and were used without further purification.

2.1. Preparation of r-BN triangular nanoplates

Into a stainless steel autoclave, 3.5 g (50 mmol) of the B_2O_3 and 4.73 g (120 mmol) of $NaNH_2$ were mixed and put. The autoclave

* Corresponding author. Fax: +86 551 3607402.

E-mail addresses: bkeyan@mail.ustc.edu.cn (K. Bao), ytqian@ustc.edu.cn (Y. Qian).

was heated to 600 °C with heating rate of 10 °C min⁻¹, maintained at 600 °C for 6 h and then cooled to room temperature naturally. The obtained white powder was filtered, washed several times with distilled water and absolute alcohol, and dried in vacuum at 60 °C for 8 h.

2.2. Characterization

Powder XRD measurements were carried out with a Philips X'Pert diffractometer (CuK α λ = 1.541874 Å; nickel filter; 40 kV, 40 mA). FESEM images were taken on a JEOL JSM-6300F SEM. TEM images, HRTEM images and SAED were performed on JEOL JEM-2010 microscope operating at 200 kV. X-ray photoelectron spectra (XPS) were recorded on a VG ESCALAB MKII X-ray photoelectron spectrometer (VG Scientific, England), using non-monochromatized MgK α radiation as the excitation source. TGA-DTA measurements were carried out on a Diamond TG/differential thermal analysis (DTA) thermal analyzer (Perkin Elmer) with a heat rate of 10 K min⁻¹ in air or N₂. Fourier transform infrared (FT-IR) spectroscopy of the sample was conducted at room temperature with a KBr pellet on a VECTOR-22 (Bruker) spectrometer ranging from 500 to 4000 cm⁻¹. PL measurements were carried out on a JY LABRAM-HR laser micro-Raman spectrometer with 514.5 nm emission lines.

3. Results and discussion

Fig. 1 shows the XRD pattern of the as-prepared product. All the reflection peaks can be indexed as r-BN, which is in good agreement with the standard data (JCPDS PDF No. 45-1171, a = 2.504 Å, c = 10.00 Å). No impurities such as B₂O₃ can be detected in the XRD pattern.

Fig. 2 displays the XPS spectrum of the as-obtained r-BN. It is found that the binding energy of B1s is at 190.1 eV, and N1s at 397.8 eV, which is consistent with the reported value of BN [27]. The qualification of the peak intensities reveals that the atomic ratio of B to N is 1:1.04, which agrees well with the chemical stoichiometric relation between B and N.

The morphology of the product was checked using FESEM and TEM. Fig. 3a is a typical FESEM image of the product, exhibiting the edge lengths of the as-obtained BN triangular nanoplates are

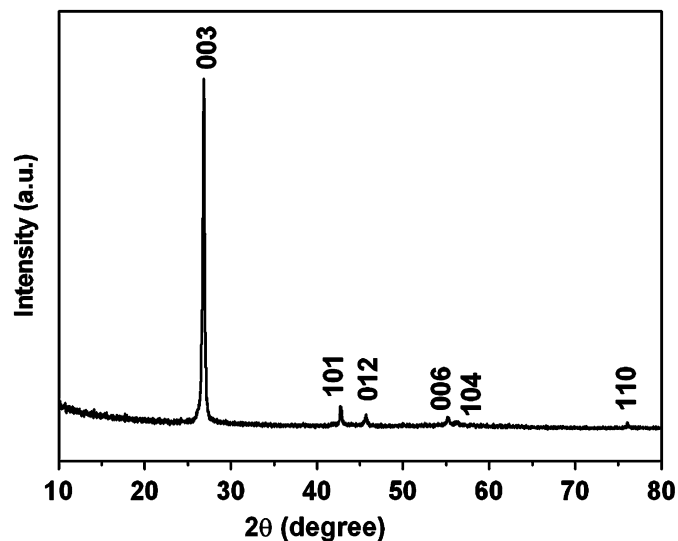


Fig. 1. XRD pattern of the as-prepared r-BN triangular nanoplates.

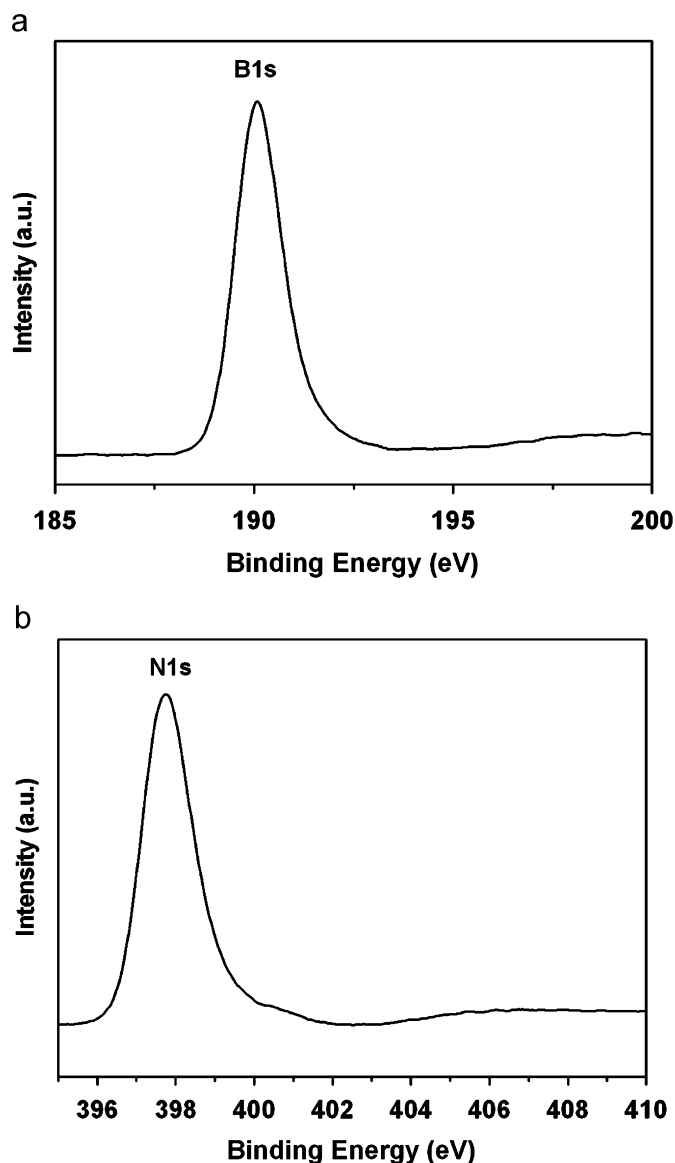


Fig. 2. XPS spectra of the as-prepared BN triangular nanoplates: (a) B1s and (b) N1s.

in the range of 300–500 nm. Fig. 3b is another typical FESEM image of the product, showing the thicknesses of the BN triangular nanoplates are about 50–90 nm. Fig. 3c is the TEM image of the product, confirming that the product is composed of triangular nanoplates about 400 nm in size.

Detailed structural analyses of the as-prepared r-BN triangular nanoplates were carried out with HRTEM and SAED. As shown in Fig. 4a, the edge length of the BN triangular nanoplate is about 380 nm. Fig. 4b exhibits the corresponding HRTEM image obtained from the square region marked b in Fig. 4a. The HRTEM image reveals that the crystal planes have lattice spacing of about 2.0 Å corresponding to (012) plane of r-BN. The corresponding SAED pattern (Fig. 4b, inset) can be indexed as (012), (104) and (1 $\bar{1}$ 2) planes of r-BN, revealing that the as-prepared product is single crystal. The thicknesses of r-BN triangular nanoplates were also recorded by TEM. As shown in Fig. 4c, the thicknesses of r-BN triangular nanoplates are about 50–80 nm. The segment in square region marked d in Fig. 4c was further investigated by HRTEM and SAED. As shown in Fig. 4d, the lattice fringes of the (003) plane with a d spacing of 3.31 Å can be clearly seen. The corresponding

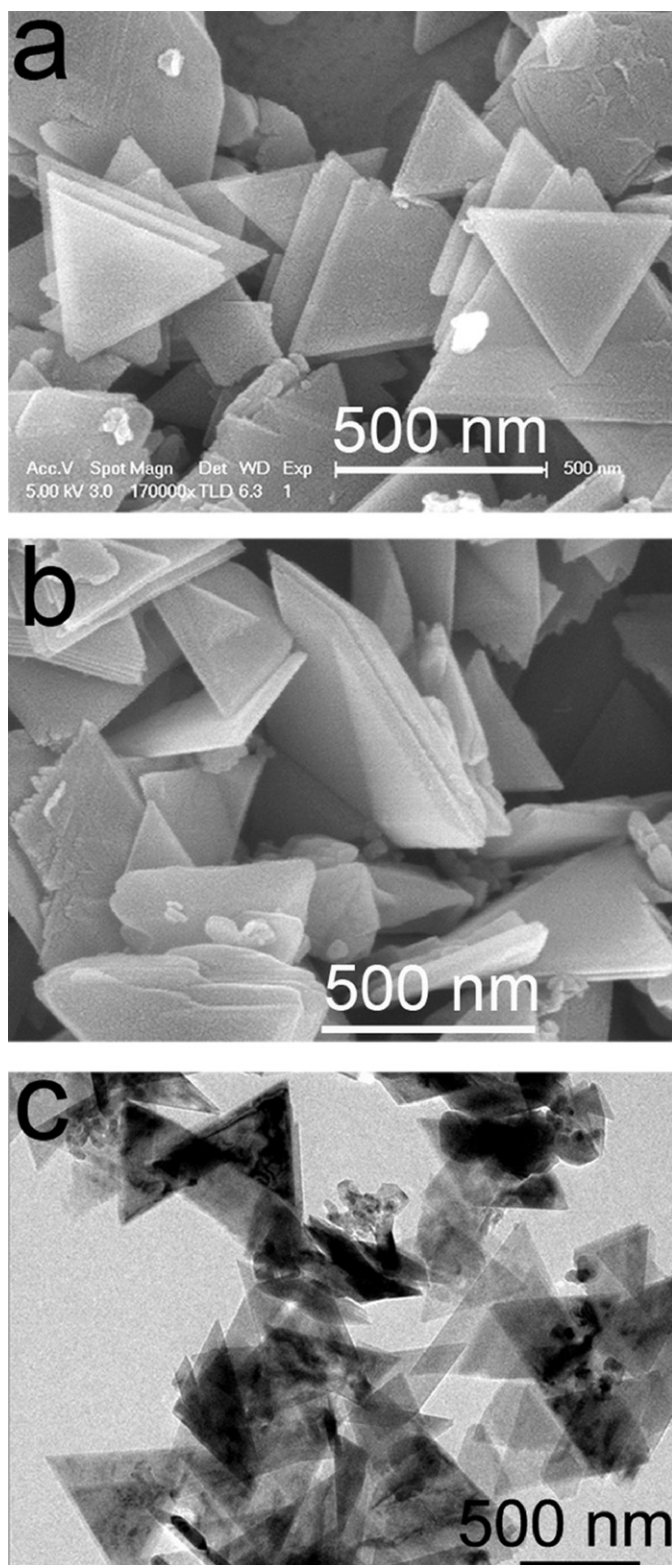


Fig. 3. (a) An overview FESEM image, (b) FESEM image showing the thicknesses and (c) TEM image of r-BN triangular nanoplates.

SAED spots (Fig. 4d, inset) can be indexed as r-BN (003), (113) and (110) planes.

Further study suggested that varying reaction temperature in the range of 550–650 °C led to no obvious change in the morphologies of r-BN products with other reaction condition unchanged. When the temperature was moderated at 550 °C, the

corresponding r-BN triangular nanoplates owned the edge lengths of 300–400 nm, while at 600 and 650 °C, the sizes augmented into about 450 and 500 nm, respectively (Fig. 5). The r-BN could not be obtained when the reaction temperature below 500 °C.

To understand the intermediate steps in the formation of r-BN triangular nanoplates, a series of controlled experiments were carried out at 600 °C for different duration of time. The XRD patterns of the products are shown in Fig. SI-1 (Supporting information), which indicate that all the products are r-BN. When the reaction time was 25 min, BN nanoparticles with a mean particles size of 50 nm were obtained (Fig. 6a). When the reaction time was prolonged to 45 min, BN nanosheets were formed (Fig. 6b). As the reaction time increased to 1 h, the morphology of the product changed remarkably. BN nanosheets gradually evolved into faceted nanoplates with sharp edges and corners (Fig. 6c). BN triangular nanoplates with edge lengths of about 200 nm were obtained at 600 °C for 2 h, although the morphology was a little irregularity and some nanoparticles were remained (Fig. 6d). Fig. 6e is a typical FESEM image of the product prepared at 600 °C for 4 h, exhibiting the product is compose of BN triangular nanoplates with edge lengths in the ranges of 300–400 nm. When the reaction time was further extended to 6 h, the morphology of the product changed slightly in contrast to the product obtained for 4 h (Fig. 6f).

Based on the above experimental results, a possible formation mechanism of the product is proposed. First, small r-BN nanoparticles were rapidly formed. The newly formed BN deposited on the formerly formed BN nanoparticles and continue to grow, and at last BN triangular nanoplates were obtained. However, we should note that the density of BN particles become gradually dilute in Fig. 6, which may be related with Ostwald ripening process, in which concentration gradients cause small precipitates to dissolve and large ones to grow. Such a similar ripening process has occurred for the preparation of other nanomaterials [28–34]. In principle, the intrinsic and extrinsic factors, the crystal structure, and the growth surroundings are accounted for in the final morphology. As we know, as for the different crystallographic faces, the growth rate is inversely proportional to the diffraction index; those crystallographic faces with low diffraction were always kept in the final products. As the final r-BN product, (003) planes have the slowest growth rate so the product exhibits nanoplate-like structure. In addition, (012), (1 $\bar{1}$ 2) and (104) planes have quick growth rate. As a result, the BN evolved into faceted nanoplates with sharp edges and corners. The growth process of BN triangular nanoplates is simply described in Scheme 1.

4. Properties

Many reports showed that the morphology, size and crystallinity of inorganic nanomaterials could greatly affect their physical and chemical properties [35–41]. To investigate the influence of morphology, size, and crystallinity on the optical property of the as-prepared r-BN, we explored the PL properties of the r-BN obtained at different reaction conditions. As shown in Figs. 7 and 8, the fluorescence intensity of r-BN is remarkably influenced by reaction temperature and time, but the peak positions of the emission spectra remain the same about 560 nm (1.9 eV). These peaks indicate that the samples have pronounced red-shift in contrast to the crystal grain or films of BN. One possible cause for this red-shift is the impurities or defects in the as-prepared BN nanostructures. Furthermore, defect luminescence of r-BN was also observed in other work [26]. Fig. 7 shows the emission spectra and emission intensity of r-BN prepared at 600 °C for different reaction times. The emission intensity of the products prepared at 600 °C for 6 h was highest, followed by 4 h,

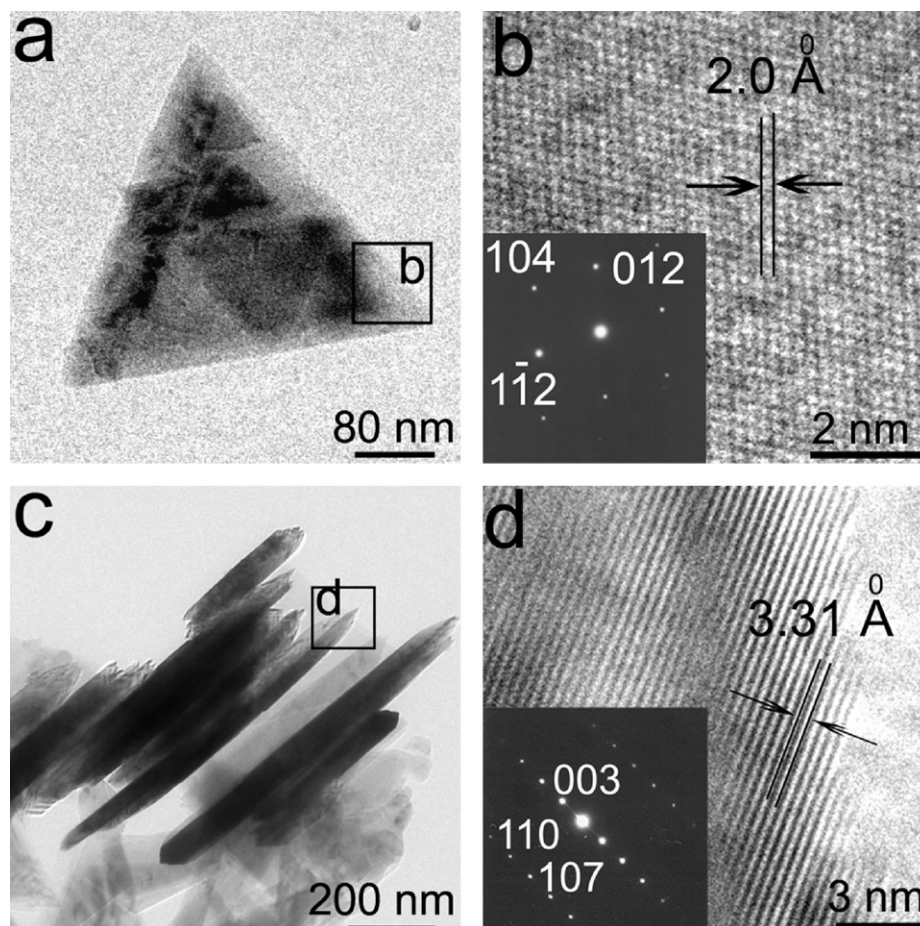


Fig. 4. (a) TEM image of an individual r-BN triangular nanoplate showing the width of BN triangular nanoplate. (b) HRTEM image obtained from the square region marked b in Fig. 4a. The inset is the corresponding SAED pattern. (c) TEM image displaying the thicknesses of BN triangular nanoplates. (d) HRTEM image obtained from the square region marked d in Fig. 4c. The inset is the corresponding SAED pattern.

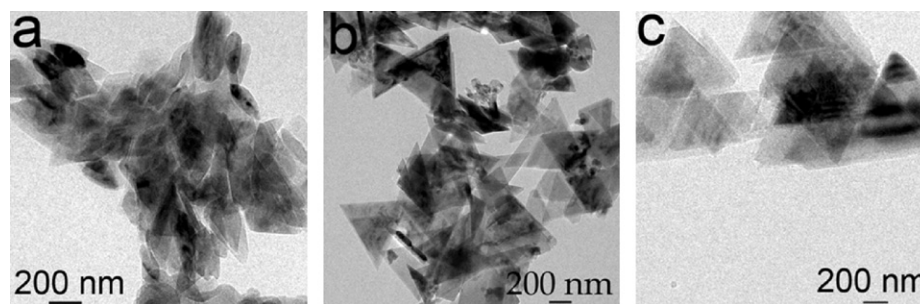


Fig. 5. TEM images of r-BN obtained at different reaction temperature for 6 h: (a) 550 °C, (b) 600 °C and (c) 650 °C.

and then 45 min. The emission intensity of the products synthesized at 600 °C for 2 h, 1 h and 25 min are similar and they are much lower than that of nanoparticles prepared for 6 h. Fig. 8 shows the emission spectra and emission intensity of BN prepared at different reaction temperature for 6 h. It can be seen that emission intensity become higher with increasing reaction temperatures. In our work, from Figs. 5, 6 and SI-1 (Supporting information) it can be seen that the morphologies, sizes and crystallinities of the products prepared at different reaction conditions changed remarkably. As we know, luminescence efficiency is increased with decreasing crystallite size and improving crystallinity, but for impurity and defect, it is always contrary. It is thought that morphology, size, crystallinity and

defect play together roles on the emission intensity of BN products.

The thermal stability of the as-prepared BN triangular nanoplates obtained at 600 °C for 6 h was examined by TGA-DTA under flowing N_2 , as shown in Fig. 9. The TGA curve (Fig. 9a) exhibits that no significant events other than a 4.75% weight loss near 100 °C, which was related to evaporation of moisture. The weight keeps nearly in balance from 100 to 1200 °C; only 0.85% weight loss happens. The DTA curve (Fig. 9b) reveals that there is no significant exothermic peak from 100 to 1200 °C. The DrTGA analysis (see Fig. SI-2, Supporting information) also indicates that the rate of weight loss has little change in the range of 100–1200 °C.

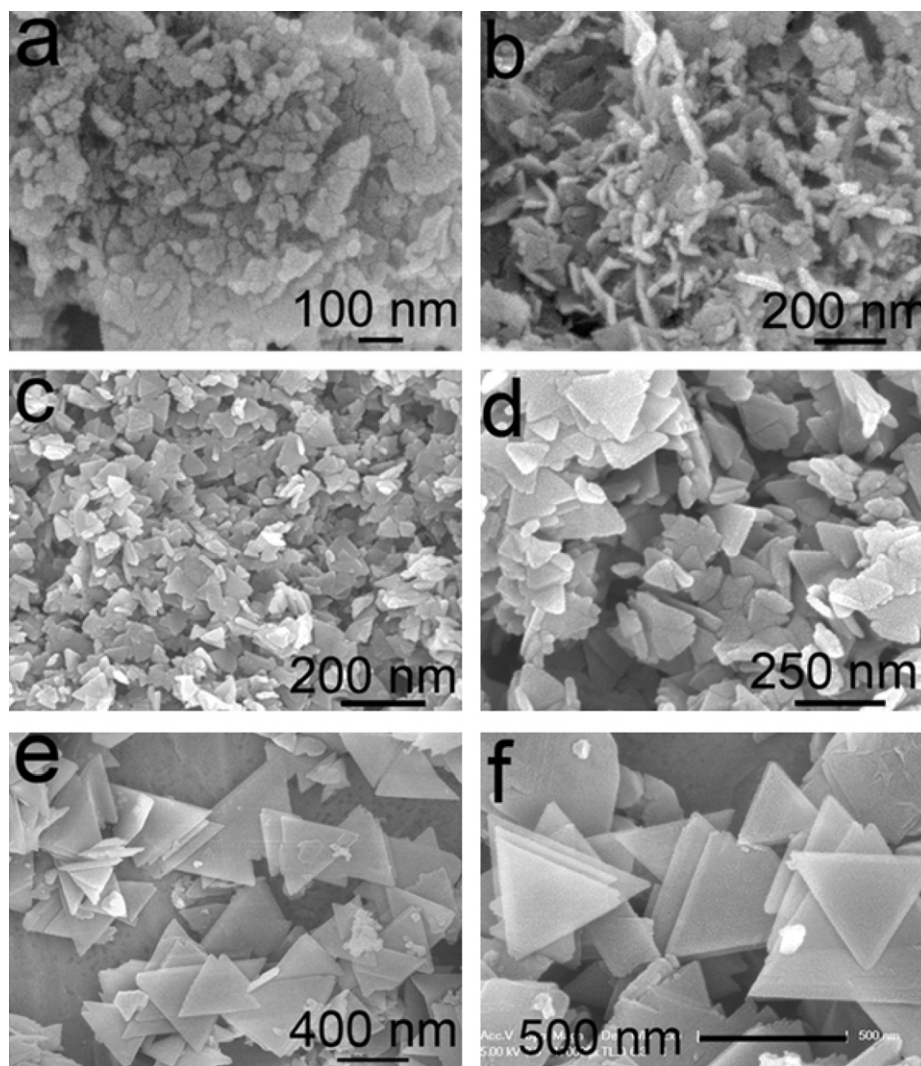
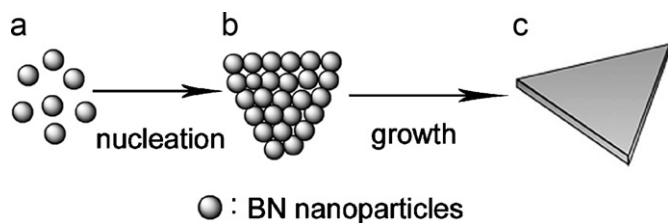


Fig. 6. FESEM images of r-BN obtained at 600 °C for different reaction time: (a) 25 min, (b) 45 min, (c) 1 h, (d) 2 h, (e) 4 h, and (f) 6 h.



Scheme 1. Schematic illustration of the formation process of BN triangular nanoplates: (a) BN nanoparticles were formed in the initial reaction process. (b) The newly formed BN deposited on the formerly formed BN nanoparticles and continued to grow. (c) At last BN triangular nanoplates was obtained.

The purity of the as-prepared r-BN triangular nanoplates was detected by Fourier transform infrared (FTIR) analysis (see Fig. SI-3, Supporting information). Two strong characteristic peaks are located at 807 and 1385 cm^{-1} , respectively. The absorption peak at 807 cm^{-1} could be attributed to the B–N–B out-of-plane bending vibration and the peak centered around 1385 cm^{-1} should be from the in-plane B–N TO modes of the sp^2 -bonded BN [42]. The broad absorption peak at 3416 cm^{-1} is due to adsorbed water on the samples. No evidences of impurities can be found. The results also confirm that the 4.75% weight loss near 100 °C in the TGA curve (Fig. 9a) is attributed to the adsorbed water on the surfaces of BN triangular nanoplates.

The TGA-DTA oxidation tests (air flow) on the as-prepared r-BN triangular nanoplates are shown in Fig. 10. From the TGA curve (Fig. 10a) it is found that the weight of the product has not changed significantly below 800 °C. From 800 to 1200 °C, the weight of the powder increases gradually by about 24.5%. As shown in the DTA curve (Fig. 10b), there is only one big exothermic peak which starts at 800 °C, ends at 1140 °C and centers at 1044 °C. Combining the results of the two curves, we can reach the following conclusions. The sample has basically not been oxidized from room temperature to 800 °C. From 800 °C on, the sample suffers gradual oxidation on its surfaces. The oxidation process becomes intensified as the temperature rises to 1044 °C, which also confirms by DrTGA curve (see Fig. SI-4, Supporting information). At the same time, a protective layer of oxide forms on the surfaces of the sample. Theoretically, the whole increment of weight is about 40% according to the calculation when BN is oxidized to B_2O_3 . But the experimental value is about 24.5%, which indicates that the BN triangular nanoplates were not completely oxidized to B_2O_3 . Previous reports showed that h-BN nanostructures are usually oxidized to B_2O_3 from 700 °C to 1000 °C [43,44]. However, the r-BN triangular nanoplates prepared in our experiment have not changed significantly below 800 °C. These reveal that the as-prepared BN has excellent thermal stability and anti-oxidation property, which may be helpful for high-temperature electro-optical applications of r-BN material.

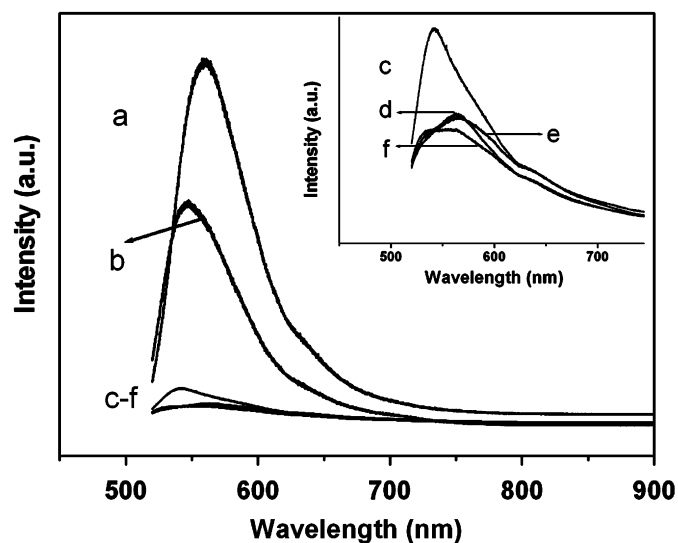


Fig. 7. PL spectra of r-BN obtained at 600 °C for different reaction time: (a) 6 h, (b) 4 h, (c) 45 min, (d) 2 h, (e) 25 min and (f) 1 h.

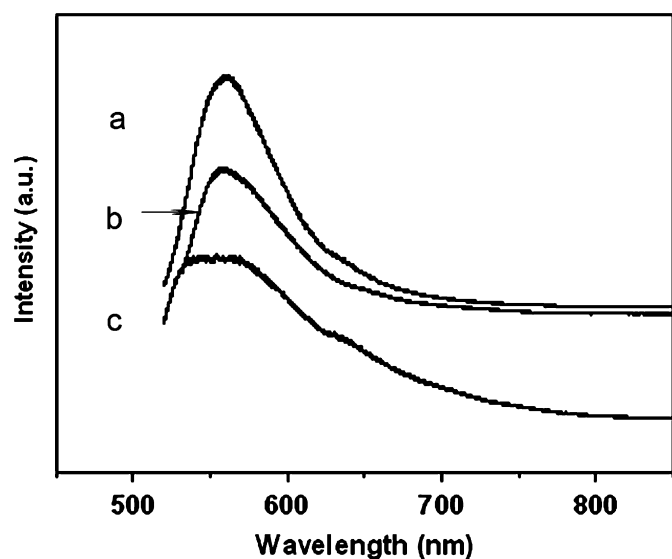


Fig. 8. PL spectra of r-BN obtained at different reaction temperature for 6 h: (a) 650 °C, (b) 600 °C and (c) 550 °C.

5. Conclusions

Highly crystalline r-BN triangular nanoplates were prepared on a large scale via a solid-state reaction at 600 °C for 6 h, in which NaNH_2 and B_2O_3 was used as reactants. An atomic ratio of B–N of 1:1.04 was determined from XPS. The widths of the as-obtained r-BN triangular nanoplates are in the ranges of 300–500 nm and the thicknesses are about 50–90 nm. TGA-DTA test under air flow showed the sample has basically not been oxidized from room temperature to 800 °C. The product was stable under N_2 flow, even if raised the temperature to 1200 °C. This means that the as-prepared r-BN has excellent thermal stability and anti-oxidation property which makes it particularly applications in high temperature devices. The results of PL measurements reveal that the r-BN products show strong yellow-green emission. Since the products exhibit excellent luminescence, they can be expected to become good candidates for research in optical and optoelectronic devices.

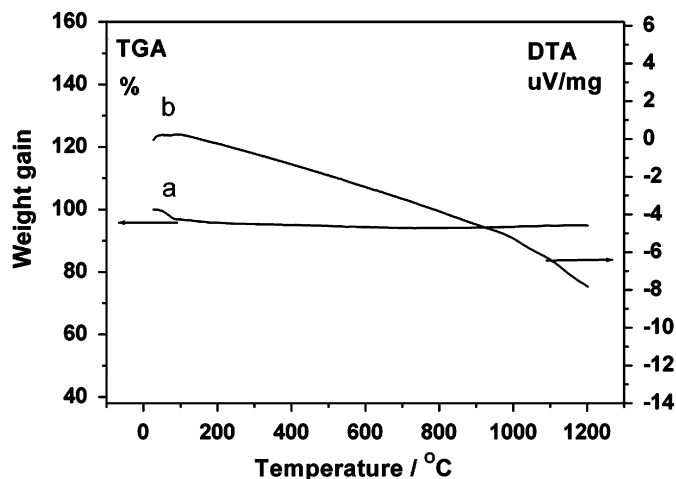


Fig. 9. (a) TGA and (b) DTA curves of the BN triangular nanoplates under flowing N_2 .

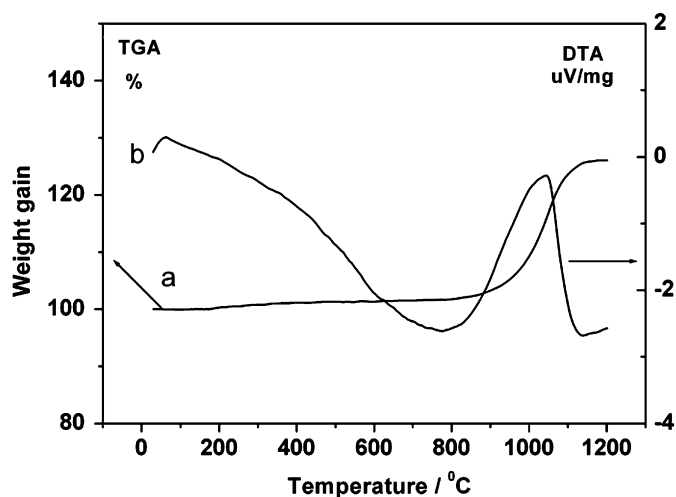


Fig. 10. (a) TGA and (b) DTA curves of the as-prepared r-BN under flowing air.

Acknowledgments

The financial support of this work, by the National Natural Science Foundation of China (no. 20431020) and the 973 Project of China (no. 2005cB623601), is gratefully acknowledged.

Appendix A. Supplementary material

Supplementary data associated with this article can be found in the online version at [doi:10.1016/j.jssc.2009.01.004](https://doi.org/10.1016/j.jssc.2009.01.004).

References

- [1] T.K. Pauli, P. Bhattacharya, D.N. Bose, *Appl. Phys. Lett.* 56 (1990) 2648.
- [2] L. Liu, Y.P. Feng, Z.X. Shen, *Phys. Rev. B* 68 (2003) (art. no. 104102).
- [3] K. Watanabe, T. Taniguchi, H. Kanda, *Nat. Mater.* 3 (2004) 404.
- [4] H. Mass, A. Currao, G. Calzaferri, *Angew. Chem. Int. Ed.* 41 (2002) 2495.
- [5] K. Watanabe, T. Taniguchi, H. Kanda, *Nat. Mater.* 3 (2004) 404.
- [6] W. Mickelson, S. Aloni, W.Q. Han, J. Cumings, A. Zettl, *Science* 300 (2003) 467.
- [7] L.Q. Xu, Y.Y. Peng, Z.Y. Meng, W.C. Yu, S.Y. Zhang, X.M. Liu, Y.T. Qian, *Chem. Mater.* 15 (2003) 2675.
- [8] T. Oku, M. Kuno, H. Kitahara, *Formation, Int. J. Inorg. Mater.* 3 (2001) 597.
- [9] T. Oku, K. Hiraga, T. Matsuda, T. Hirai, M. Hirabayashi, *Diamond Relat. Mater.* 12 (2003) 1918.

- [10] X.J. Wang, Y. Xie, Q.X. Guo, Chem. Commun. (2003) 2688.
- [11] L.Y. Chen, Y.L. Gu, L. Shi, Z.H. Yang, J.H. Ma, Y.T. Qian, Solid State Commun. 130 (2004) 537.
- [12] F. Xu, Y. Xie, X. Zhang, S.Y. Zhang, X.M. Liu, X.B. Tian, Inorg. Chem. 43 (2004) 822.
- [13] L. Shi, Y.L. Gu, L.Y. Chen, Z.H. Yang, J.H. Ma, Y.T. Qian, Mater. Lett. 58 (2004) 3301.
- [14] M.T. Zheng, Y.L. Gu, Z.L. Xu, Y.L. Liu, Mater. Lett. 61 (2007) 1943.
- [15] X.W. Zhang, H.G. Boyen, N. Deyneka, P. Ziemann, F. Banhart, M. Schreck, Nat. Mater. 2 (2003) 312.
- [16] J.B. Wang, G.W. Yang, C.Y. Zhang, X.L. Zhong, Z.H.A. Ren, Chem. Phys. Lett. 367 (2003) 10.
- [17] H.H. Jiang, K. Li, L.G. Gai, Q.L. Wang, D.L. Cui, M.H. Jiang, J. Mater. Sci. Technol. 23 (2007) 768.
- [18] H. Koga, T. Miyazaki, S. Watanabe, T. Ohno, Jpn. J. Appl. Phys. 43 (2004) 4092.
- [19] J. Guo, H. Wang, J.S. Zhu, K. Zheng, M.K. Zhu, H. Yan, M. Yoshimura, Electrochem. Commun. 9 (2007) 1824.
- [20] R.H. Wentorf, J. Chem. Phys. 26 (1957) 956.
- [21] X. Wang, Y.H. Yang, G.W. Yang, Appl. Phys. Lett. 84 (2004) 3034.
- [22] C.X. Wang, G.W. Yang, Mater. Sci. Eng. R 49 (2005) 157.
- [23] T. Oku, K. Hiraga, T. Matsuda, T. Hirai, M. Hirabayashi, Diamond Relat. Mater. 12 (2003) 1138.
- [24] S.D. Yuan, X.X. Ding, Z.X. Huang, X.T. Huang, Z.W. Gan, C. Tang, S.R. Qi, J. Cryst. Growth 256 (2003) 67.
- [25] C.C. Tang, Y. Bando, T. Sato, K. Kurashima, Chem. Commun. (2002) 1290.
- [26] L.Q. Xu, J.H. Zhan, J.Q. Hu, Y.S. Bando, X.L. Yuan, T. Sekiguchi, M. Mitome, D. Golberg, Adv. Mater. 19 (2007) 2141.
- [27] T. Goto, T. Hirai, J. Mater. Sci. 7 (1988) 548.
- [28] H.G. Yang, H.C. Zeng, J. Phys. Chem. B 108 (2004) 3492.
- [29] B. Liu, H.C. Zeng, Small 1 (2005) 566.
- [30] X.W. Lou, Y. Wang, C. Yuan, J.Y. Lee, L.A. Archer, Adv. Mater. 18 (2006) 2325.
- [31] K.Y. Bao, S.Z. Liu, J. Cao, J.B. Liang, Y.C. Zhu, X.B. Hu, L.L. Zhu, X.Y. Liu, Y.T. Qian, J. Nanosci. Nanotechnol. 9 (2009) 1.
- [32] B.X. Li, G.X. Rong, Y. Xie, L.F. Huang, C.Q. Feng, Inorg. Chem. 45 (2007) 6404.
- [33] H.B. Li, L.L. Chai, X.Q. Wang, X.Y. Wu, G.C. Xi, X.Y. Liu, Y.T. Qian, Cryst. Growth. Des. 7 (2007) 1918.
- [34] G.F. Zou, H. Li, D.W. Zhang, K. Xiong, C. Dong, Y.T. Qian, J. Phys. Chem. B 110 (2006) 1632.
- [35] R. Agarwal, C.M. Lieber, Appl. Phys. A 85 (2001) 209.
- [36] L.P. Liu, Q. Peng, Y.D. Li, Inorg. Chem. 47 (2008) 3182.
- [37] C.M. Cobley, D.J. Campbell, Y.N. Xia, Adv. Mater. 20 (2008) 748.
- [38] B.D. Yuhas, D.O. Zitoun, P.J. Pauzauskie, R. He, P.D. Yang, Angew. Chem. Int. Ed. 45 (2006) 420.
- [39] N. Tian, Z.Y. Zhou, S.G. Sun, Y. Ding, Z.L. Wang, Science 316 (2007) 732.
- [40] L. Shi, Y.M. Xu, S.K. Hark, Y. Liu, S. Wang, L.M. Peng, K.W. Wong, Q. Li, Nanoletters 7 (2007) 3559.
- [41] W.W. Zhou, K.B. Tang, S.U. Zeng, Y.X. Qi, Nanotechnology 19 (2008) 065602.
- [42] C.D. Wagner, W.M. Riggs, L.E. Davis, J.F. Moulder, G.E. Muilenberg, Handbook of X-ray Photoelectron Spectroscopy, Physical Electronics Division, Perkin-Elmer Corporation, Eden Prairie, Minnesota, 1979.
- [43] Z.H. Yang, L. Shi, L.Y. Chen, Y.L. Gu, P.J. Cai, A.W. Zhao, Y.T. Qian, Chem. Phys. Lett. 405 (2005) 229.
- [44] J.H. Ma, J. Li, G.X. Li, Y.G. Tian, J. Zhang, J.F. Wu, J.Y. Zheng, H.M. Zhuang, T.H. Pan, Mater. Res. Bull. 42 (2007) 982.